Electronic Supplementary Information (ESI)

A bee pupa-infilled honeycomb structure-inspired Li_2MnSiO_4 cathode for high volumetric energy density secondary batteries

Jinyun Liu,*[,a] Xirong Lin,[b] Huigang Zhang,[c] Zihan Shen,[c] Qianqian Lu,[b] Junjie Niu,[d,*] Jinjin Li,[b,*] and Paul V. Braun[e,f,g,*]

[a] *Key Laboratory of Functional Molecular Solids, Ministry of Education, College of Chemistry and Materials Science, Anhui Normal University, Wuhu, Anhui 241002, P.R. China. E-mail: jyliu@iim.ac.cn*

[b] *Key Laboratory for Thin Film and Micro Fabrication, Ministry of Education, Department of Micro/Nano Electronics, Shanghai Jiao Tong University, Shanghai 200240, P.R. China. Email: lijinjin@sjtu.edu.cn*

[c] *National Laboratory of Solid State Microstructures, Nanjing University, Nanjing 210093, P.R. China* [d] *Department of Materials Science and Engineering, University of Wisconsin-Milwaukee, Milwaukee, Wisconsin 53211, USA. E-mail: niu@uwm.edu*

[e] *Department of Materials Science and Engineering,* [f] *Department of Chemistry,* [g] *Frederick Seitz Materials Research Laboratory, University of Illinois at Urbana-Champaign, Urbana, Illinois 61801, USA. E-mail: pbraun@illinois.edu*

Experimental details and modelling methods

PS opal template fabrication

The PS opal template was fabricated on a tungsten foil (≥99.9% trace metals basis, 8 mm × 18 mm × 0.2 mm) which was a chemically stable and mechanically robust substrate. The PS spheres with a diameter of 630 nm (Shanghai Qifa Biotech Co., Ltd) were first dispersed in de-ionized water to form a 0.1 wt.% suspension. Then the pre-cleaned W was placed vertically into a plastic vial that contains the PS suspension at 60 °C for 12 h. Finally, the opal template was formed after heating at 95 °C for 3 h.

Porous Li_2MnSiO_4/C scaffold preparation

At first, a solution A was prepared by dissolving CH_3COOLi and $Mn(CH_3COO)_2$ with a stoichiometric ratio into 50 wt.% acetic acid followed by adding 1.0 g of glucose. Another solution B of 0.01 mol of tetraethylorthosilicate (TEOS) and 16 mL isopropanol was added drop by drop under stirring, forming the Li_2MnSiO_4/C sol. The PS template was vertically immersed into the Li_2MnSiO_4/C sol for 2 s and then dried naturally. After that, the sample was sintered in a tube furnace at 700 °C (Heating rate: 3 °C min^{-1}) for 8 h under H_2/Ar (H_2: 5 vol.%) gas. All the chemicals were purchased from Sinopharm Chemical Reagent Co., Ltd, and used without further purification.

3D BPFH-shaped Li_2MnSiO_4/C synthesis

Before the Li_2MnSiO_4/C particles was embedded into the 3D Li_2MnSiO_4/C scaffold, a SiO_2 layer was coated on the scaffold using a Stöber method. In a typical experiment, 8 mL of de-ionized water and 2 mL of ammonium hydroxide were mixed with 40 mL of ethanol. Then

the W substrate with Li_2MnSiO_4/C scaffold was hung on by a clamp and immersed into the obtained solution vertically. 1 mL TEOS was added dropwise into the solution under magnetic stirring. After 1.5 h, the sample was taken out, washed and dried. Then the SiO_2coated Li_2MnSiO_4/C was vertically immersed into the fresh Li_2MnSiO_4/C sol again. After 4 h, it was collected and dried overnight. The sample was subsequently treated at 700 °C for 8 h under H_2/Ar (H_2: 5 vol.%) gas. Finally, the obtained sample was immersed in a 5% HF aqueous solution for 1.5 h to remove the SiO_2 layer.

Characterization

The morphology, structure and composition of the samples were characterized using SEM (FEI QUANTA 200FEG, operated at 15 kV), HRTEM (JEOL JEM-2010, operated at 200 kV), and XRD (Philips X'Pert) with a high intensity Cu Kα radiation at 1.54178 Å, respectively. The carbon ratio within the Li_2MnSiO_4/C composite was analyzed using Raman microscopy (LabRAM HR800) and thermal gravimetric analysis-differential scanning calorimetry (TGA-DTG-60H) in air atmosphere with a heating rate of 10 °C min^{-1} from 25 °C to 800 °C. Elemental mappings were performed on the HRTEM equipped with an Oxford INCA energy-dispersive X-ray (EDX) analyzer. The elemental states were identified by X-ray photoelectron spectroscopy (XPS, Thermo-VG Scientific ESCALAB 250).

Electrochemical measurements

The electrochemical performance of the prepared samples was measured using a CR2032 coin cell system. The Li_2MnSiO_4/C cathode or the TiO_2 anode was used as the working electrode. For the half cell, lithium metal was used as the counter electrode; for the full cell

with Li_2MnSiO_4/C, commercial graphite was used as the anode electrode. 1.0 M $LiPF_6$ in a mixture of EC: DEC (1:1, vol%) as the electrolyte. All cells were assembled in an Ar-filled glove box (Mikrouna Super 1220/750, O_2 and H_2O levels < 0.01 ppm). The electrochemical performance was tested using a galvanostatic discharge/charge method on a Neware battery tester (Shenzhen Neware Technology Co., Ltd, CT-4008). Electrochemical impedance spectroscopy (EIS, 0.01-100 kHz) was recorded on an electrochemical workstation (CHI660D). CV curves were recorded on the same electrochemical workstation at a scan rate of

0.1 mV s^{-1}. The cycling capability of the battery at –5 °C and 50 °C was performed inside a high-low temperature chamber (DSP-HT, Shenzhen Disi Equipment Co., Ltd). The coin cells were first stored in the chamber at –5 °C or 50 °C for 24 h before the battery test. During the electrochemical measurement, the chamber was kept at a constant temperature of –5 °C and 50 °C, respectively.

DFT calculations

The first-principle calculations using a CASTEP program were performed with the generalized gradient approximation (GGA) of Perdew-Burke-Ernzerhof (PBE) and the GGA+U approximation as implemented in Material Studio package. A kinetic energy cut-off value of 600 eV for plane wave basis was adopted for all DFT computations. Brillouin zone integrations were performed with the *k*-points sampled using Monkhorst–Pack (MP) grids of 3×3×3 and 3×3×1 for bulk Li_2SiMnO_4 and slab Li_2SiMnO_4 (100) calculations, respectively.

The convergence criteria were set to 10^{-5} eV and 0.03 eV $Å^{-1}$ for the electronic self-consistent iteration and the forces on each atom, respectively. To address onsite coulomb interactions in the localized d electrons of transition-metal ions, Hubbard parameter correction was conducted (U_{Mn}=6.0 eV).

Mechanical property modeling

The first-principles calculation is to study the electron structures and properties, and to understand the important physical and chemical properties of materials by solving the Schrodinger equation of multi-particle system. Therefore, the first-principles calculation has advantages in efficient searching of stable structures and identification of electrochemical parameters, such as the calculations of tensile strength after the lattice distortion of a material. In our investigation, we performed the first-principles calculations using the VASP code, with the energy cutoff for a plane wave basis set of 500 eV. The pseudopotential was prefixed with the Projector-Augmented wave (PAW) method, the exchange interactions between ions and electrons was described by the Generalized Gradient Approximation (GGA), and the exchange correlation energy density was described by Perdew-Burke-Ernzerhof (PBE). The plane wave truncation energy was set to be 400 eV, the convergence criterion of the total energy calculation was 1 x 10^{-6}, where the standard of convergence was that the force between atoms is less than 1 x 10^{-2} eV/ Å.

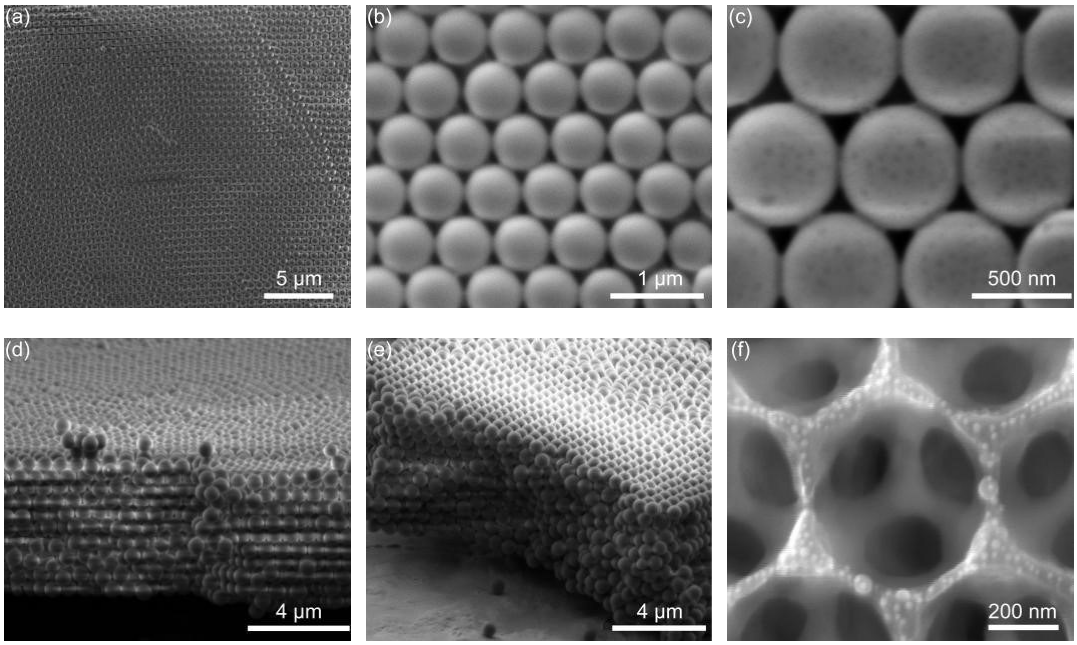

Fig. S1. (a-c) Top-view SEM images of the PS opal template. (d-e) Cross-sectional SEM images and (f) high-magnification top-view SEM image of the 3D Li_2MnSiO_4/C scaffold.

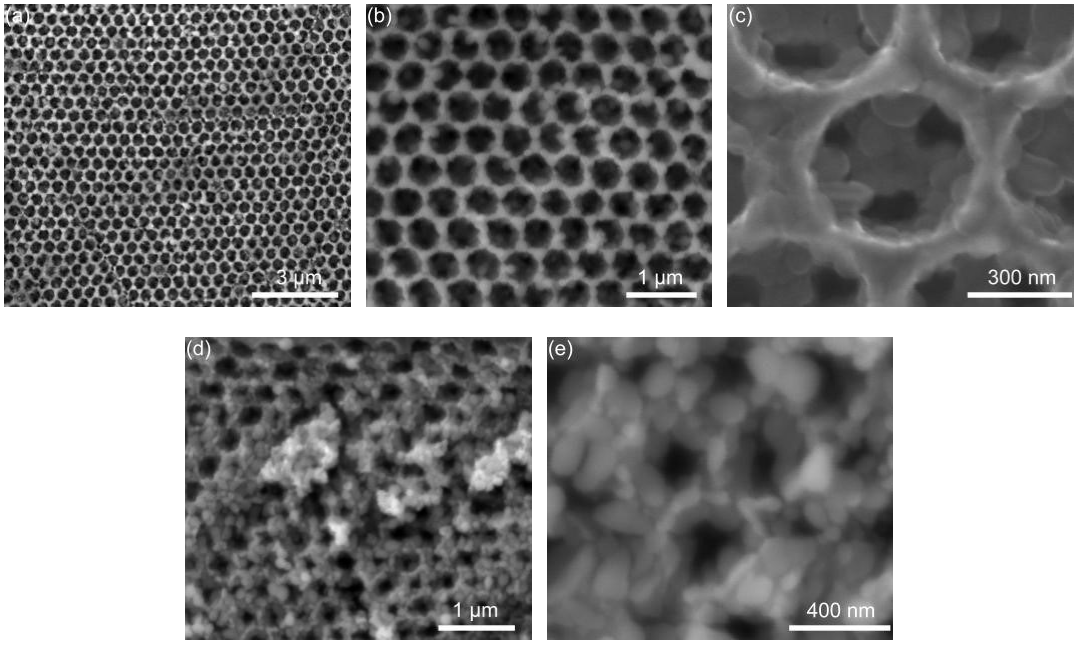

Fig. S2. (a-c) Top-view, and (d-e) cross-sectional SEM images of the SiO_2-coated Li_2MnSiO_4/C scaffold.

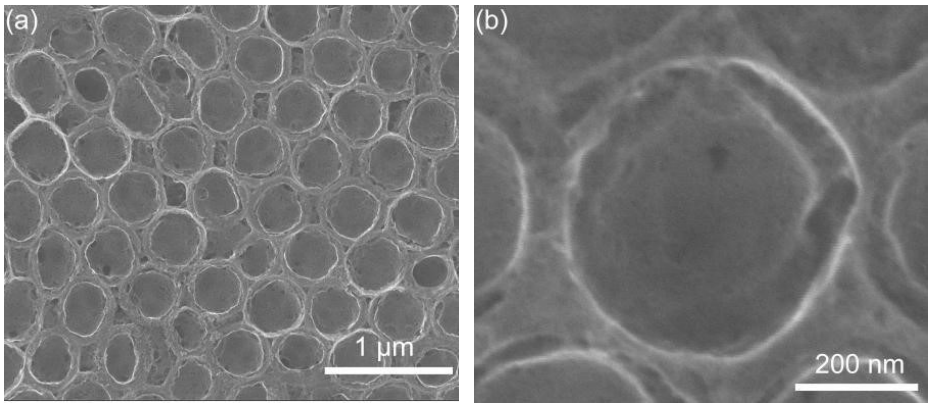

Fig. S3. (a) Low- and (b) high-magnification SEM images of the 3D BPFH-shaped Li_2MnSiO_4/C composite.

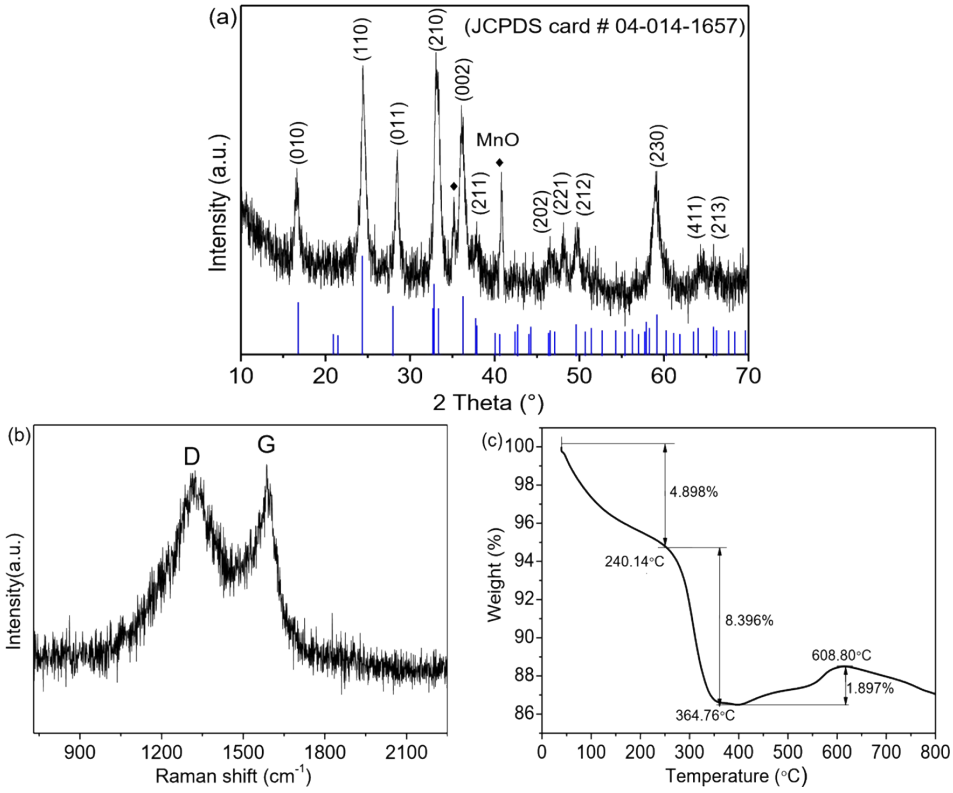

Fig. S4. (a) XRD pattern, (b) Raman spectrum and (c) TGA curve of the 3D BPFH-shaped Li_2MnSiO_4/C. In (a), the blue lines present the peaks and their positions of the XRD pattern in JCPDS card # 04-014-1657.

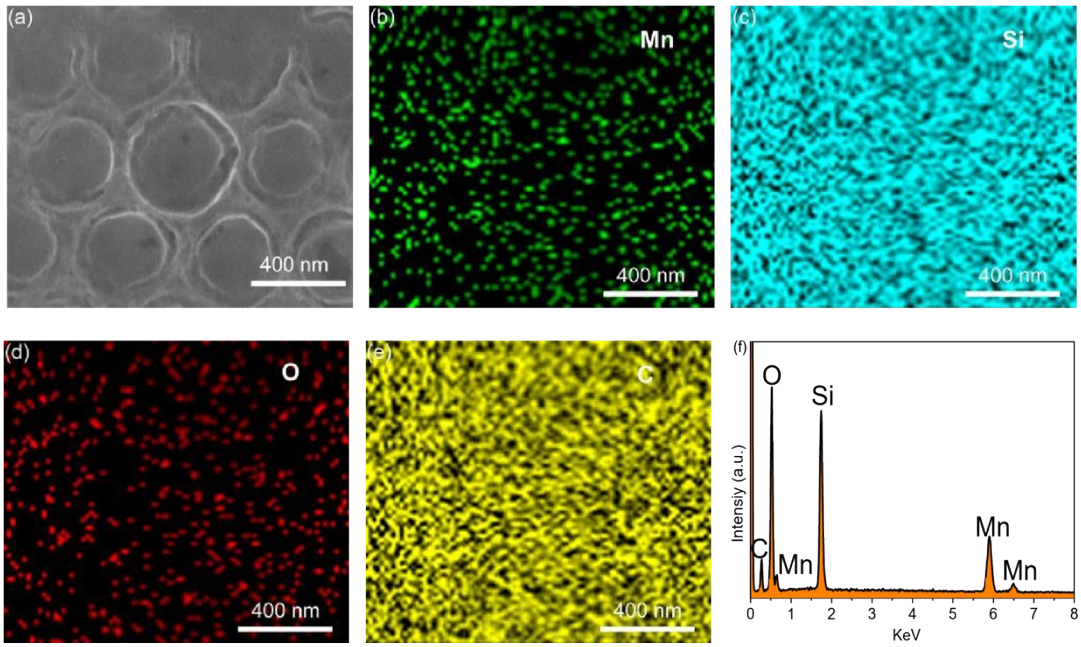

Fig. S5. SEM image (a) and the corresponding elemental mappings of (b) Mn, (c) Si, (d) O, and (e) C of the 3D BPFH-shaped Li_2MnSiO_4/C. (f) The EDX spectrum.

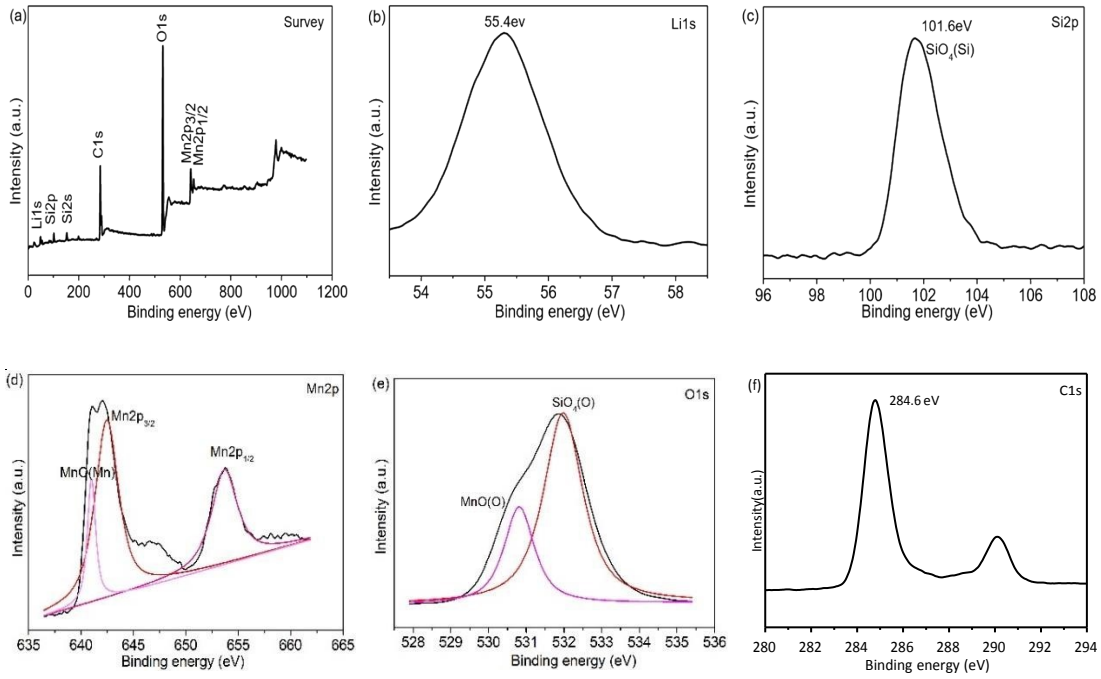

Fig. S6. XPS spectra of the 3D BPFH-shaped Li_2MnSiO_4/C composite. High-resolution XPS spectra of (b) Li 1s, (c) Si 2p, (d) Mn 2p, (e) O 1s, and (f) C 1s.

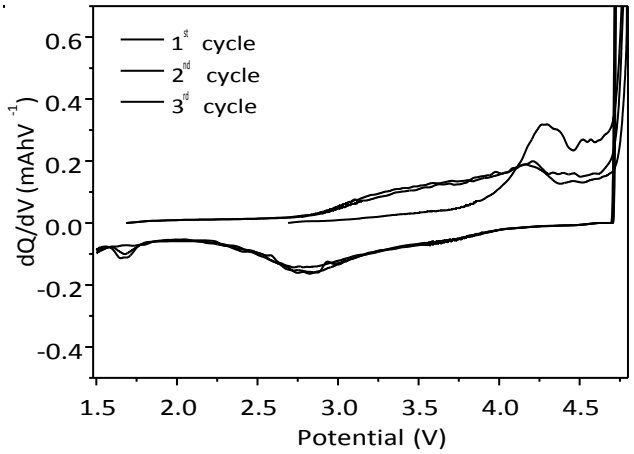

Fig. S7. The differential capacities *vs* potential (dQ/dV) plots of the BPFH-shaped Li_2MnSiO_4/C cycling at 0.1C over the potential window of 1.5–4.8 V.

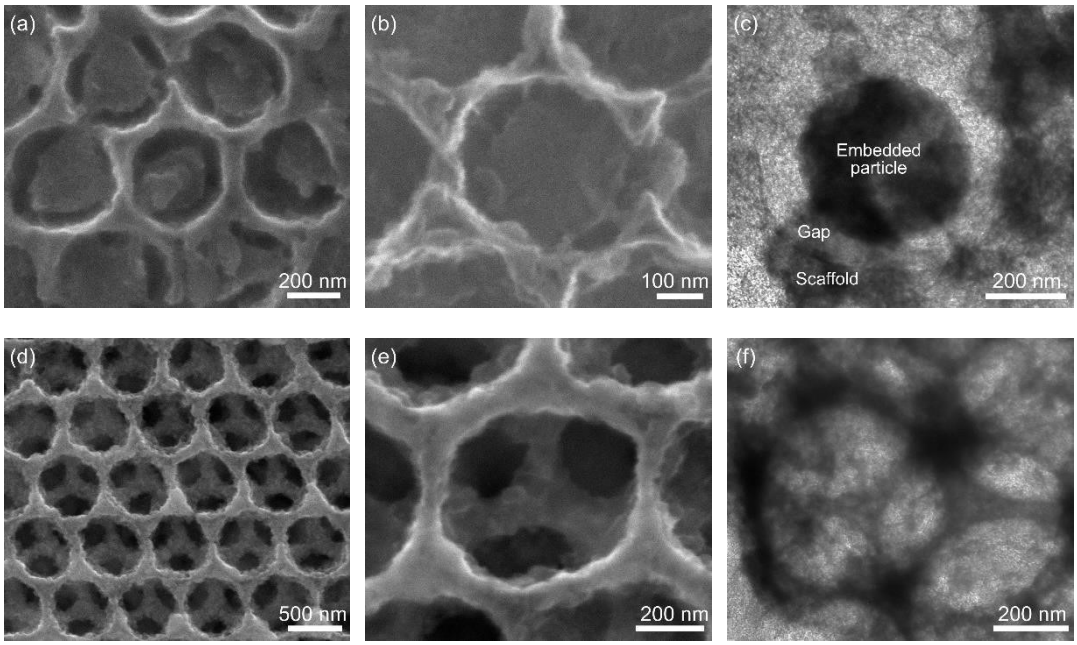

Fig. S8. (a-b) SEM and (c) TEM images of the BPFH-shaped Li_2MnSiO_4/C after cycling at 0.1C for 100 times. (d-e) SEM and (f) TEM images of the post-cycled 3D Li_2MnSiO_4/C scaffold without particles filling.

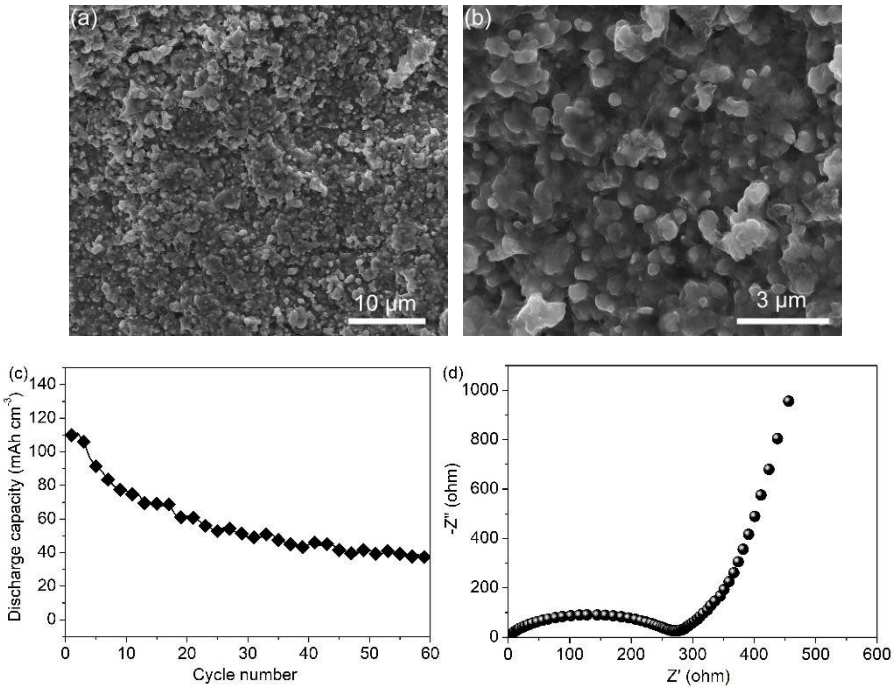

Fig. S9. (a) Low- and (b) high-magnification SEM images of the Li_2MnSiO_4/C thin film. (c) Cycling performance of the thin film at 0.1C between 1.5 and 4.8 V. (d) Nyquist plots of the Li_2MnSiO_4/C thin film-based fresh cell. For the preparation of Li_2MnSiO_4/C thin film, the same procedure as the 3D BPFH-shaped Li_2MnSiO_4/C was used except no PS template.

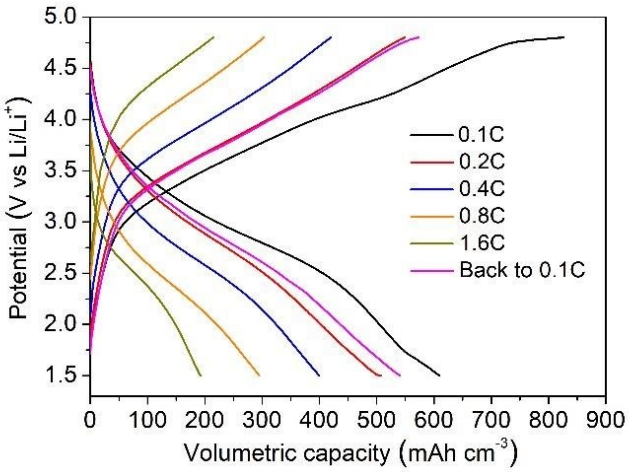

Fig. S10. Galvanostatic charge/discharge profiles of the 3D BPFH-shaped Li_2MnSiO_4/C cathode at a series of rates from 0.1 to 1.6C.

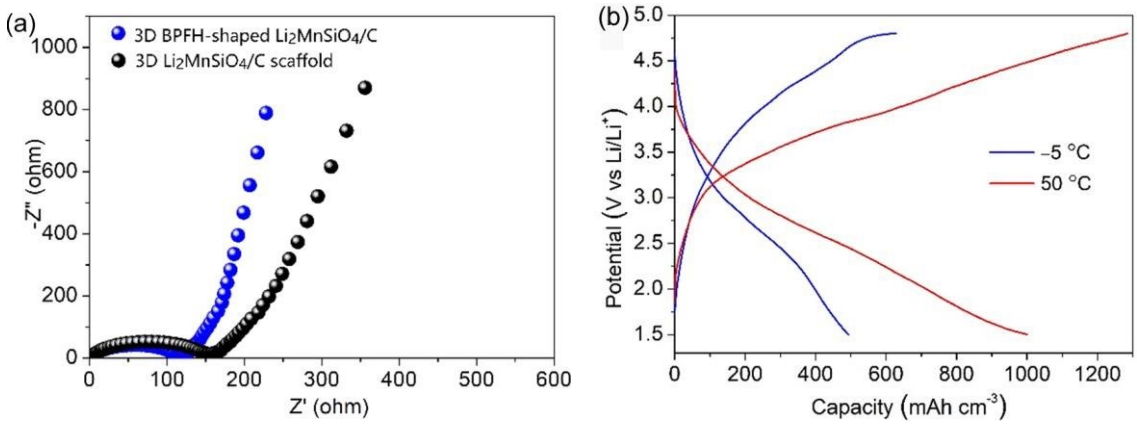

Fig. S11. (a) Nyquist plots of the 3D Li_2MnSiO_4/C with or without embedded Li_2MnSiO_4/C particles. (b) Charge/discharge curves of the 3D BPFH-shaped Li_2MnSiO_4/C cathode under temperatures of –5 ºC and 50 ºC at a rate of 0.1C. Through the electrochemical impedance spectroscopy results in (a), the Li ion diffusion coefficients were calculated. At first, the Warburg coefficient σ_w can be obtained by the equation: $Z = R_e + R_{ct} + \sigma_w\omega^{-1/2}$, where ω is the angular frequency in the low frequency region, R_e and R_{ct} are kinetics parameters independent of frequency. The Z exhibits a linear relationship with $\sigma_w^{-1/2}$. Then, the Li ion diffusion coefficient is calculated by equation: $D_{Li^+} = {}_2$ $A^2n^R{}_4{}^2F^T{}_4{}^2C^2\sigma^{w2}$, where R is the gas constant (8.314 J mol^{-1} K^{-1}), T is the temperature (298 K), A is the area of electrode, F is the

Faraday's constant (96500 C mol^{-1}), and C is the molar concentration of Li ion.

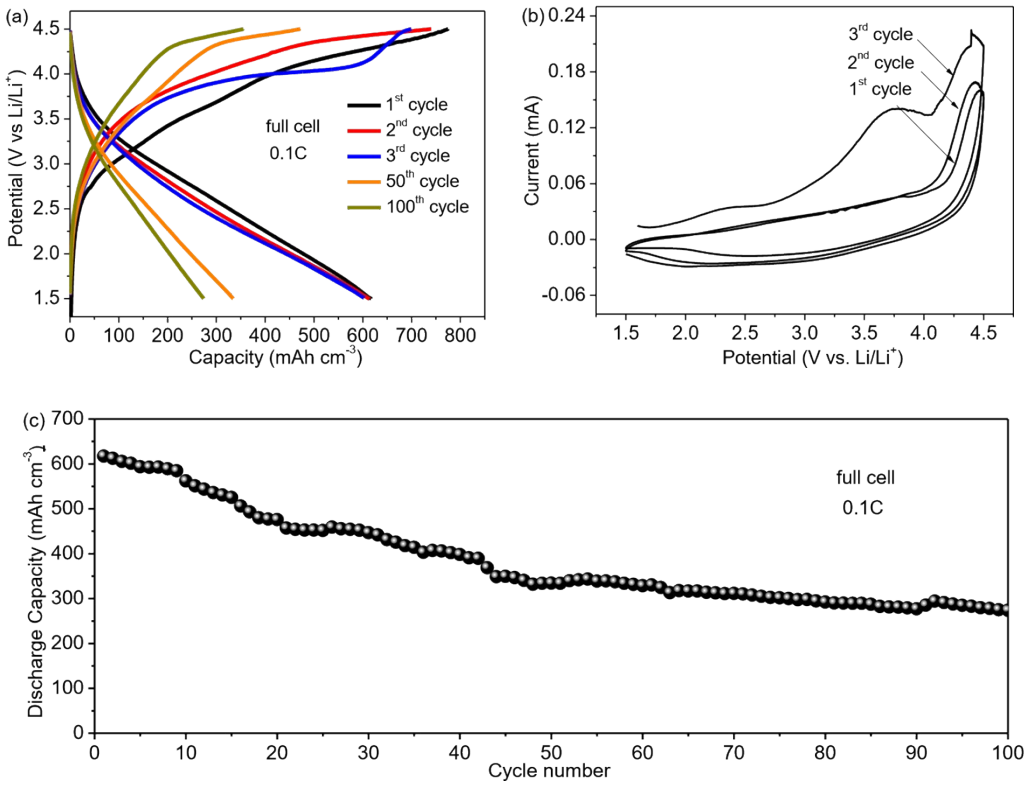

Fig. S12. Electrochemical performance of the full cell battery using the 3D BPFH-shaped Li_2MnSiO_4/C as cathode *vs* commercial graphite as anode. (a) Galvanostatic charge/discharge curves at 0.1C from 1.5 to 4.5 V. (b) CV curves over the potential range of 1.5−4.5 V *vs* Li/Li^+ at a scan rate of 0.1 mV s^{-1}. (c) Cycling performance at 0.1C. The discharge capacity was calculated on the basis of the cathode electrode.

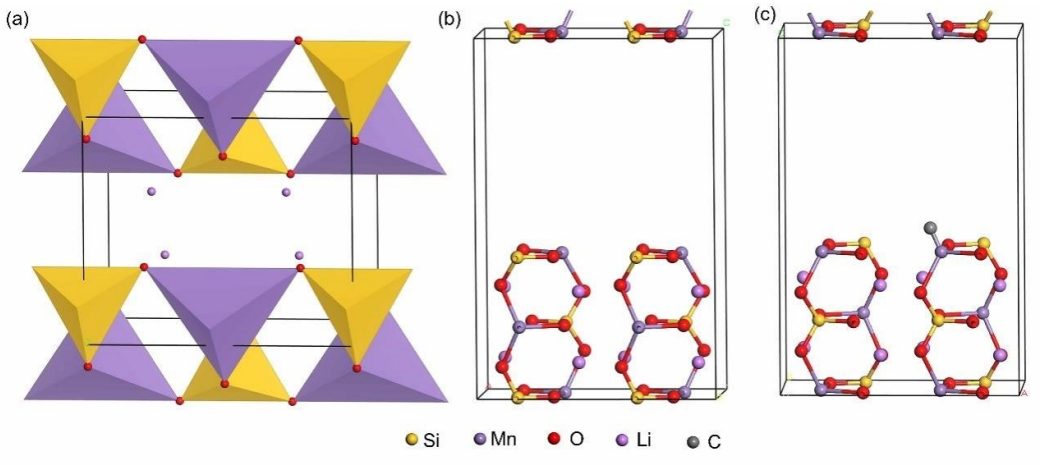

Fig. S13. Slab models of the (a) Li_2MnSiO_4 with a $Pmn2_1$ space group, (b) Li_2MnSiO_4 (100) surface, and (c) Li_2MnSiO_4 (100)/C.

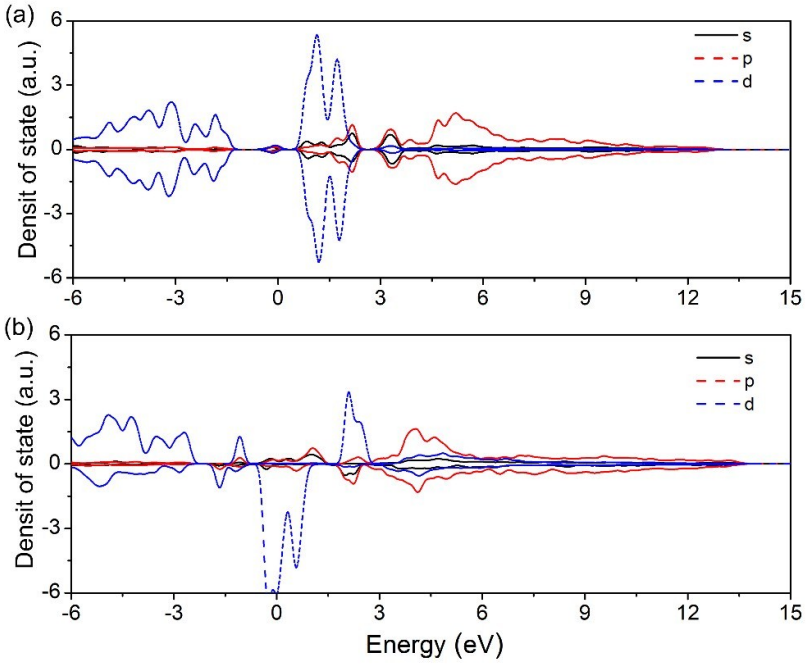

Fig. S14. The PDOS of orbits s, p, d of the Mn atom in the Li_2MnSiO_4 (100) surface (a) before and (b) after coating with carbon.

Table S1. Comparison of the volumetric capacity with various cathodes.

Composition	Potential vs. Li/Li^+ (V)	Rate	Cycle number	Volumetric capacity ($mAh\ cm^{-3}$)	Ref.
Low temperature-sintered $LiFePO_4$	3.5	0.2C	1	340	1
			40	296	
Carbon-PPy	3.4	1C	1	53	2
$LiMnPO_4$	~3.9	0.05C	1	263	3
			50	257	
$LiFePO_4$ arbon-coated	3.5	0.1C	1	225	4
			500	218	
$LiFePO_4$	3.5	0.1C	1	325	5
$LiCoO_2$	4.0	0.1C	1	90	6
3D Li_2MnSiO_4/C scaffold without particles inside	4.2, 4.5	0.1C	1	362	This work
			100	102	
3D BPFH-shaped Li_2MnSiO_4/C	4.2, 4.5	0.1C	1	643	This work
			100	316	

C

Table S2. Comparison of the gravimetric capacity with Li_2MnSiO_4-based cathodes.

Structure	Preparation method	Rate	Cycle number	Gravimetric capacity ($mAh\ g^{-1}$)	Ref.
Li_2MnSiO_4/C particles	PVA assisted solgel method	0.03C	100	21	7
$Li_2Mn_{1-x}Ni_xSiO_4$/C (5% Ni doped)	Hydrothermal route	0.05C	30	64	8

MoO_2-coated Li_2MnSiO_4/C	Sol-gel	1C	20	70	9
Li_2MnSiO_4/C	Ultrasoundassisted synthesis	0.2C	50	56	10
ZnO-coated Li_2MnSiO_4/C	Sol-gel	0.5C	25	71	11
Li_2MnSiO_4/C	*In-situ* synthesis	30 mA g^{-1}	40	70	12
$Li_2Mn_{1-x}Mo_xSiO_4$/C (6% Mo doped)	Sol-gel	0.1C	20	61	13
Li_2MnSiO_4/C film	Sol-gel	0.2C	50	50	14
Li_2MnSiO_4/C film	Sol-gel	0.05C	16	48	15
Li_2MnSiO_4/C film	Sol-gel	0.05C	20	67	16
Li_2MnSiO_4/C spheres	Microwave-assisted sol-gel	0.1C	50	48	17
3D BPFH-shaped Li_2MnSiO_4/C	Templated method	0.1C	100	102	This work

Table S3. Crystal structures and the parameters in Brillouin zone.

Phase	x	y=x/(1+x)	a	b	c	k-points
Mn_2SiO_4	0	0	4.955	6.348	10.772	9 × 7 × 5
$LiMnSiO_4$	1	0.5	4.915	6.401	9.035	9 × 7 × 5
$Li_3Mn_2(SiO_4)_2$	1.5	0.6	5.102	10.616	6.688	9 × 5 × 7
$Li_5Mn(SiO_4)_2$	5	0.714	7.265	7.607	6.358	7 × 7 × 7
Li_4SiO_4	∞	1	5.232	5.387	6.143	7 × 7 × 7

References

1 J. H. Seo, J. Guo, H. Z. Guo, K. Verlinde, D. S. B. Heidary, R. Rajagopalan, C. A.

Randall, *Ceram. Int.* 2017, **43**, 15370.

2 S. W. Woo, K. Dokko, K. Kanamura, *J. Power Sources* 2008, **185**, 1589.

3 N. H. Kwon, H. Yin, T. Vavrova, J. H. W. Lim, U. Steiner, B. Grobety, K. M. Fromm, *J. Power Sources* 2017, **342**, 231.

4 S. W. Oh, S. T. Myung, S. M. Oh, C. S. Yoon, K. Amine, Y. K. Sun, *Electrochim. Acta* 2010, 55, 1193.

5 P. K. Shen, H. L. Zou, H. Meng, M. M. Wu, *Funct. Mater. Lett.* 2011, **4**, 209.

6 E. C. Self, E. C. McRen, R. Wycisk, P. N. Pintauro, Electrochim. Acta 2016, 214, 139.

7 N. Wagner, A. M. Svensson, F. Vullum-Bruer, *Solid State Ionics* 2015, **276**, 26.

8 H. Deng, S. X. Zhao, X. Wu, L. Wei, Y. F. Deng, C. W. Nan, *RSC Adv.* 2016, **6**, 111539.

9 J. T. Zhu, H. Q. Tang, Z. Y. Tang, C. X. Ma, Q. Xu, X. H. Zhang, *Electrochim. Acta* 2015, **16**, 183.

10 C. Hwang, T. Kim, J. Shim, K. Kwak, K. M. Ok, K. K. Lee, *J. Power Sources* 2015, **294**, 522.

11 J. T. Zhu, H. Q. Tang, Z. Y. Tang, C. X. Ma, *J. Alloy. Compd.* 2015, **633**, 194.

12 D. Sun, H. Y. Wang, P. Ding, N. Zhou, X. B. Huang, S. Tan, Y. G. Tang, *J. Power Sources* 2013, **242**, 865.

13 C. Y. Lai, Z. Wang, Q. J. Xu, H. X. Li, *Mater. Lett*. 2015, **139**, 134.

14 S. Won, K. K. Lee, G. Park, H. J. Sun, J. C. An, J. Shim, *J. Appl. Electrochem.* 2015, **45**, 169.

15 S. Devaraja, M. Kuezmaa, C. T. Nga, P. Balayaa, *Electrochim. Acta* 2013, **102**, 290.

16 Q. Q. Zhang, Q. C. Zhuang, S. D. Xu, X. Y. Qiu, Y. L. Cui, Y. L. Shi, Y. H. Qiang, *Ionics* 2012, **18**, 487.

17 J. J. Choi, S. Kim, W. B. Im, W. Chang, B. W. Cho, J. H. Kim, H. L. Choi, K. Y. Chung, *J. Electroceram.* 2013, **31**, 176.